Research Article

Journal of PeptideScience

Received: 5 January 2010 Revised: 22 February 2010 Accepted: 23 February 2010 Published online in Wiley Interscience: 6 April 2010

(www.interscience.com) DOI 10.1002/psc.1230

Study on structure and assembly of the third transmembrane domain of Slc11a1

Shuyan Xiao, Yuxia Wang, Lei Yang, Haiyan Qi, Chunyu Wang and Fei Li*

The structure and self-assembly of the peptide corresponding to the third transmembrane domain (TMD3) of Slc11a1 and its E139A mutant are studied in 1,1,1,3,3,3-hexafluoro-2-propanol (HFIP) aqueous solution by NMR and CD experiments. Slc11a1 is an integral membrane protein with 12 putative TMDs and functions as a pH-coupled divalent metal cation transporter. Glu139 of Slc11a1 is highly conserved within predicted TMD3 of the Slc11 protein family and function-associated. Here, we provide the first direct experimental evidence for the structural features of two 24-residue peptides corresponding to TMD3 of Slc11a1 and its E139A mutant in 60% HFIP-d_2 aqueous solution using CD and NMR spectroscopies. Our study shows that the membrane-spanning peptide folds as a typical amphipathic α-helix structure from Ile5 to Met20 with hydrophilic residues Glu12 (Glu139 in Slc11a1) and Asp19 lying on the same side of the helix. The substitution of Glu139 by an alanine residue has little effect on the structure of the peptide, but increases hydrophobicity and facilitates self-assembly of the peptide. Although the wildtype peptide is monomeric in HFIP aqueous solution, the E139A mutant forms a dimer. The increase in hydrophobicity of the membrane-spanning peptide and/or change in the interactions between transmembrane segments induced by E139A mutation may affect the metal ion transport of the protein. Copyright © 2010 European Peptide Society and John Wiley & Sons, Ltd.

Keywords: Slc11a1-TMD3; E139A; structure; assembly; NMR

Introduction

The solute carrier family 11 member 1 (Slc11a1, formerly named as natural resistance-associated macrophage protein 1, Nramp1) belongs to a family of proton-coupled transporters that facilitate the cellular absorption of divalent metal ions [1]. It is an integral membrane phosphoprotein and is expressed exclusively in late endosomal/lysosomal compartment of macrophages as well as in polymorphonuclear leukocytes [2–5]. Slc11a1 includes 12 transmembrane domains (TMDs), a glycosylated extracellular loop, and several phosphorylation sites [6]. It is crucial for normal functioning of cells. Defective Slc11a1 causes susceptibility to infection by several intracellular pathogens including *Mycobacterium, Leishmania*, and *Salmonella* and is implicated in a number of diseases known as autoimmune or inflammatory diseases [5,7].

In the Slc11 protein family, Slc11a2 (Nramp2, DCT1) and MntH were widely studied. Slc11a2 shares 64% amino acid identity with Slc11a1 and has a broad substrate range including Fe^{2+}, Zn^{2+}, Co^{2+}, Mn^{2+}, Cu^{2+}, Cd^{2+}, Ni^{2+}, and Pb^{2+} [8–10]. MntH is the bacterial homolog of Slc11 and plays a role in manganese acquisition [11–14]. It was demonstrated that the Slc11 family possesses a common topological TM organization and higher conservation. The metal ion transport of Slc11 is driven by a proton electrochemical gradient and dependent on extraoocytic pH. The maximal transport was found at pH 5.5 [15,16]. The mutations in many corresponding sites of Slc11a2 and MntH caused similar change in the function of these proteins [1]. Both naturally occurring mutations, G185R of Slc11a2 that causes anemia and G169D of Slc11a1 that increases susceptibility to intracellular pathogen infection, were found in the neighboring position of the TMD4 (position 185 in Slc11a2 corresponds to position 170 in Slc11a1) [17–19]. It is inferred that the Slc11 homologs may have similar transport mechanism and some conservative residues or motifs of Slc11 homologs may play similar role in the function of these proteins.

In the TMDs of Slc11 proteins, TMD3 were found to be important for specific aspects of transport. The mutation from Glu to Ala at position 154 (E154A) within the putative TMD3 of Slc11a2 caused complete loss of function [1,20]. Similar results were also found in MntH, the conservative mutations of E102D and E102Q (Glu102 is analogous to Glu154 in Slc11a2 and Glu139 in Slc11a1) resulted in a complete loss of transport activity [14]. The conservative mutations of D109E, D109N, E112D, and E112Q in TMD3 of MntH showed partial loss of transport function. On the basis of the effects of mutations on Mn^{2+} transport, Haemig and Brooker proposed a model for the binding of Mn^{2+} to MntH in which the residues Asp34 and Asn37 in TMD1 and Asp109 and Glu112 in TMD3 (and possibly other residues) are involved in the coordination of Mn^{2+} [14].

To understand the functions of Slc11 proteins at a molecular level, it is crucial to determine their three-dimensional structures on the atomic resolution. Because of the difficulties in the determinations of the integral membrane proteins, we selected isolated peptides from individual putative TMDs of Slc11 proteins to simulate the behavior of the TM segments in the integral membrane proteins. Although the interactions among TMDs were sacrificed, the structural information of a TMD could still be achieved by isolated peptide. In the beginning of this study, we tried to use sodium dodecyl sulfate (SDS) and

* *Correspondence to: Fei Li, State Key Laboratory of Supramolecular Structure and Materials, Jilin University, 2699 Qianjin Avenue, Changchun 130012, People's Republic of China. E-mail: feili@jlu.edu.cn*

State Key Laboratory of Supramolecular Structure and Materials, Jilin University, Changchun 130012, People's Republic of China

dodecylphosphocholine (DPC) micelles as membrane mimics. Unfortunately, we could not obtain well-solved NMR spectra owing to severe signal overlap even after changing several experimental conditions (temperature, pH value, concentration, and ionic strength). In this case, we used 1,1,1,3,3,3-hexafluoro-2-propanol (HFIP) aqueous solution as membrane-mimetic medium to investigate the structure of the peptide. It has long been known that 2,2,2-trifluoroethanol (TFE) and HFIP can induce formation of helical conformations of peptides as their physical and chemical properties resemble those of a biomembrane. Therefore, the fluoric alcohols have been widely employed to simulate hydrophobic environments and to establish the *in vivo* conformations of many peptides that either reside within or are bound to membranes [21–25].

Materials and Methods

Materials

Two peptides with the sequences of Lys-Val-Pro-Arg-Ile-Leu-Leu-Trp-Leu-Thr-Ile-**Glu**-Leu-Ala-Ile-Val-Gly-Ser-Asp-Met-Gln-Glu-Val-Ile and Lys-Val-Pro-Arg-Ile-Leu-Leu-Trp-Leu-Thr-Ile-**Ala**-Leu-Ala-Ile-Val-Gly-Ser-Asp-Met-Gln-Glu-Val-Ile, corresponding to the TMD3 of the wildtype Slc11a1 (WT) and its E139A mutant (E139A), were synthesized by Biopeptide Company (San Diego, CA, USA). The purity was assessed by HPLC and mass spectroscopy to be >95%. The deuterated reagent HFIP-d_2 (98%) was purchased from Cambridge Isotope Laboratories. The solvent HFIP (99.5%) was purchased from Acros Organics. All chemicals were used as purchased directly without further purification.

CD Experiments

The CD spectra were obtained on a Jasco J-810 spectropolarimeter using 0.5 mm path length cuvettes at room temperature. The peptide was dissolved in 0.3 ml HFIP solvent and then 0.2 ml water was added to arrive at a final concentration of 20 μM. The CD spectra were recorded over the wavelength range of 260–190 nm with bandwidth 1.0 nm, data pitch 0.1 nm, sweep speed 50 nm min^{-1}, and a response time 0.25 s. Three spectra per sample were acquired and averaged, followed by subtraction of the CD signal of the solvent. The secondary structure contents were estimated by the CDPro software package using the program CONTINLL with a 56-protein set.

NMR Experiments

NMR experiments were carried out on a Bruker Avance 500 MHz spectrometer at 310 K. A 5-mm triple resonance inverse probe (TBI) with *z*-gradient coil was used. A certain amount of peptide was solubilized in 0.3 ml HFIP-d_2 solvent and then 0.2 ml water was added in the peptide/HFIP-d_2 mixture to obtain a final sample of 2 and 0.5 mM peptide in 60% HFIP-d_2 aqueous solution for NMR measurement. Two-dimensional NOESY experiments were recorded with mixing time of 200 ms, transients of 48–104, data points of 2048 in *F*2 dimension and 512 in *F*1 dimension. Two-dimensional TOCSY experiments were performed with mixing time of 100 ms, transients of 44–56, data points of 2048 in *F*2 dimension and 512 in *F*1 dimension. Water suppression was achieved using WATERGATE technique. The spectra were processed using XWINNMR software (version 3.5) and NMR assignments were obtained using Sparky software [26]. The proton chemical shifts were referenced to TSP [sodium salt of 3-(trimethylsilyl)-propionate-2,2,3,3-d_4].

Structure Calculation

The structural calculation of the peptides was performed using the program CYANA (version 1.0.6) [27]. A total of 20 structures with the lowest target function values of NMR constraints were selected from 200 calculated structures and further refined by energy minimization employing the AMBER7 force field [28–30]. The check for the stereo-chemical quality of the peptide structure and achievement of Ramachandran angles for the 20 energy-minimized structures were carried out using PROCHECK-NMR software [31]. Three-dimensional structures were displayed with MOLMOL software [32].

DOSY Spectra

The diffusion ordered spectroscopy (DOSY) experiments were carried out at 298 K with bipolar pulse pair stimulated echo (BPPSTE) sequence using WATERGATE for water suppression. The diffusion time (Δ) was 50 ms and the length of the gradient pulse (δ) was 8.6 ms for WT and 10.6 ms for E139A to let the signal decay go down to 5%. The pulse gradient (g) was incremented in 16 steps ranging between 2% and 95% of the maximum gradient in a linear ramp and the data were acquired with 8 scans. The diffusion measurement of H_2O was carried out using sequence of pulsed field gradient stimulated echo (STE) without water suppression for viscosity calibration. The Δ was set to 50 ms and δ was set to 5.2 ms for WT and 5.8 ms for E139A, respectively, with scans of 8. The diffusivities of both 2 and 0.5 mM samples were measured by DOSY experiments.

Calculation of Apparent Molecular Mass from the Translational Diffusion Coefficient

In a small spherical particle, the relationship between the self-diffusion coefficient (D) and the viscosity is given by the Stokes–Einstein equation:

$$D = k_B T / 6\pi \eta r_H \quad (1)$$

where k_B is the Boltzmann constant, T the absolute temperature, η the viscosity and r_H the hydrodynamic radius. D_{HFIP/H_2O}, the diffusion coefficient of water in 60% HFIP-d_2 aqueous solution containing peptide, was measured to determine the viscosity of this solution. Assuming that the hydrodynamic radius of water remains unchanged in both pure water and 60% HFIP-d_2 aqueous solution containing peptide, the viscosity of 60% HFIP-d_2 aqueous solution, η_{HFIP/H_2O}, can be obtained as follows:

$$\eta_{HFIP/H_2O} = D_{H_2O}\eta_{H_2O} / D_{HFIP/H_2O} \quad (2)$$

where the diffusion coefficient of pure water, D_{H_2O}, is 2.272×10^{-9} m^2 s^{-1} [33] and viscosity, η_{H_2O}, is 0.890×10^{-3} N s m^{-2} [34].

Through η_{HFIP/H_2O} and D_P (the diffusion coefficient of peptide in 60% HFIP-d_2 aqueous solution), the molecular mass (M) was derived from the following equation:

$$M = \left(K_B T / 6\pi \eta_{HFIP/H_2O} F D_P\right)^3 \left[4\pi N_A / 3(\nu_2 + \delta_1 \nu_1)\right] \quad (3)$$

where F is the shape factor, for protein shapes modeled as rotational ellipsoids, a value of 1.0325 was used [35]. N_A is Avogadro's number, ν_2 (7.8×10^{-4} m^3 kg^{-1} based on the amino acid composition) [36] and ν_1 (6.7×10^{-4} m^3 kg^{-1}) [37] are the

Journal of PeptideScience

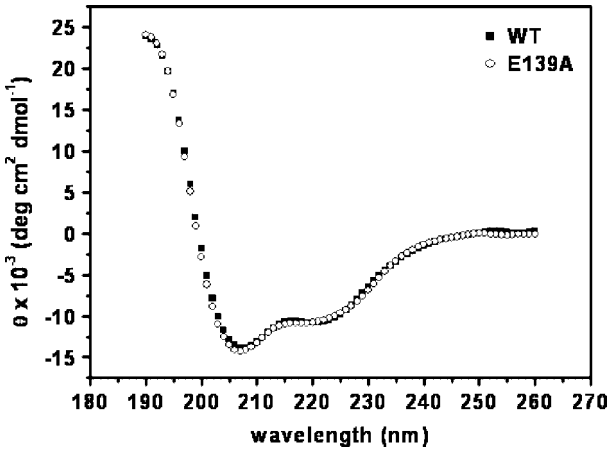

Figure 1. CD spectra of 20 μM WT peptide and E139A mutant at room temperature.

partial specific volumes of the peptide and solvent molecule, respectively, and δ_1 is the fractional amount of water bound to the molecule (hydration number), generally in the range of 0.3–0.4 g H_2O per gram of protein for most proteins [38]. For short peptides like those in the current study, which probably have fewer 'buried' groups than proteins, the hydration number might be expected to be in the upper end of this range [35]. So in this study, we used a value of 0.4 for δ_1.

Results and Discussion

CD Spectra

The conformation of the WT peptide and its E139A mutant in 60% HFIP aqueous solution were investigated by CD spectroscopy. The CD spectra of both peptides are very similar to each other, displaying typical α-helical characters with double minima at 207 and 222 nm and a positive band at 192 nm (Figure 1). The contents of α-helix, β-stand, turn and unordered structure, determined by CONTINLL software from CDPro package are 38.6%, 11.6%, 18.9%, and 30.9%, respectively, for the WT peptide, and 37.1%, 14.0%, 19.1%, and 29.8%, respectively, for the E139A mutant.

NMR Structures

The NOESY spectra of the WT peptide and the E139A mutant were well dispersed in the presence of 60% HFIP-d_2. Full and unambiguous assignments of spin systems and sequential resonances were performed by combined use of two-dimensional TOCSY and NOESY spectra. A series of short-range connectivities of H$\alpha(i)$-HN$(i+1)$ and HN(i)-HN$(i+1)$ and medium-range connectivities of H$\alpha(i)$-HN$(i+3)$, H$\alpha(i)$-HN$(i+4)$, and H$\alpha(i)$-H$\beta(i+3)$ in the NOESY spectra of WT peptide (Figure 2(A) and (B)) are diagnostic of the presence of helical structure. A total of 226 nonredundant distance constraints resulting from 403 NOE cross-peaks in the NOESY spectrum were used in the structure calculation, the 20 structures with the lowest target functions were further optimized by energy minimization using AMBER7 force field. No NOE violations larger than 0.2 Å and no dihedral angle violations larger than 5° were observed in any of the 20 structures. The CYANA calculation based on these NOE restraints gave an α-helical structure spanning from Ile5 to Met20 for the WT peptide. In the helical structure, both charged residues Glu12 and Asp19 locate on the same side and hydrophobic residues occupy the opposite side, displaying an amphipathic character. An ensemble and mean structure of the 20 lowest target function structures are shown in Figure 3 and the structural statistics are summarized in Table 1. Segments of amphipathic helices are a common structure feature found in integral membrane proteins that function as ion channels. It plays important roles in stabilization of protein–protein and protein–lipid interactions, and these interactions promote the ordered assembly and oligomerization of membrane proteins [39]. The apolar face would interact with the hydrophobic lipid bilayer and the polar face may be involved in the formation of transmembrane channel/pore either by self-assembly of several monomers or by organization of several homologous domains [40] and the hydrophilic sidechains of residues from the polar face point to the interior of the pore. In ionic channels and transporters, such conserved charged residues on the polar face can mediate interactions with aqueous solvent or with substrate molecules, participate in the process of ion permeation, account for the cation selectivity, modulate the opened or closed state of a channel, and form ionic bridges important for interhelix packing [39,41,42].

Lam-Yuk-Tseung *et al.* found that mutations at Glu154 in Slc11a2 (corresponding to Glu139 in Slc11a1) resulted in a complete loss of function [20]. Therefore, the structure of the E139A mutant of Slc11a1-TMD3 in 60% HFIP-d_2 aqueous solutions were also determined by NMR at the temperature of 310 K for comparison. The fingerprint region of the NOESY spectrum of E139A mutant showed clear medium-range connectivities H$\alpha(i)$-HN$(i+3)$, H$\alpha(i)$-HN$(i+4)$, and H$\alpha(i)$-H$\beta(i+3)$ from Arg4 to Met20 (Figure 2(C) and (D)), revealing an α-helical segments over this range. A total of 239 nonredundant distance constraints resulting from 423 NOE cross-peaks in the NOESY spectrum were used for the structure calculation. The CYANA calculation gave an α-helical structure spanning from Ile5 to Asp19 for the E139A mutant (Figure 3). The first four and the last five residues were disordered.

Figure 3 shows that the two peptides adopt similar folding in HFIP-d_2 aqueous solution and the substitution of Ala for Glu at position 12 (139 in Slc11a1) has little effect on the peptide structure. This is also supported by the CD data. The similarity of the two peptides in structure is also evidenced by Hα chemical shifts that show few differences for the two peptides (Figure2(B) and (D)). Whereas the Hα chemical shifts are closely associated with the secondary structure of a peptide, the HN chemical shifts are more correlated to the surrounding environment of the peptide. Figure 4 shows that the HN chemical shifts of the E139A mutant are significantly up-field shifted mainly in the region from the *N*-terminus to Ala14 (Lys128-Ala141 in Slc11a1) while keeping the resonances of the *C*-terminal residues less changed. This implies that the segment from the *N*-terminus to Ala14 in the mutated peptide is surrounded by more hydrophobic environment than the WT peptide, i.e. the E139A substitution results in an increase in the hydrophobicity of the peptide. The difference in the hydrophobicity of the two peptides can be seen from their surface potential (Figure 5). The increased hydrophobicity associated with the Glu → Ala substitution might either enhance the tendency of aggregation or change topology of the membrane-spanning segment. It has been proved that increased hydrophobicity impairs the transport activity of a channel, for example, ORAI1 channel. Mutations of the amino acid arginine at position 91 of ORAI1 with more hydrophobic residues led to a change in pore size and thus a reduction or complete abolishment of current activation, whereas Arg91 mutations with hydrophilic amino acids

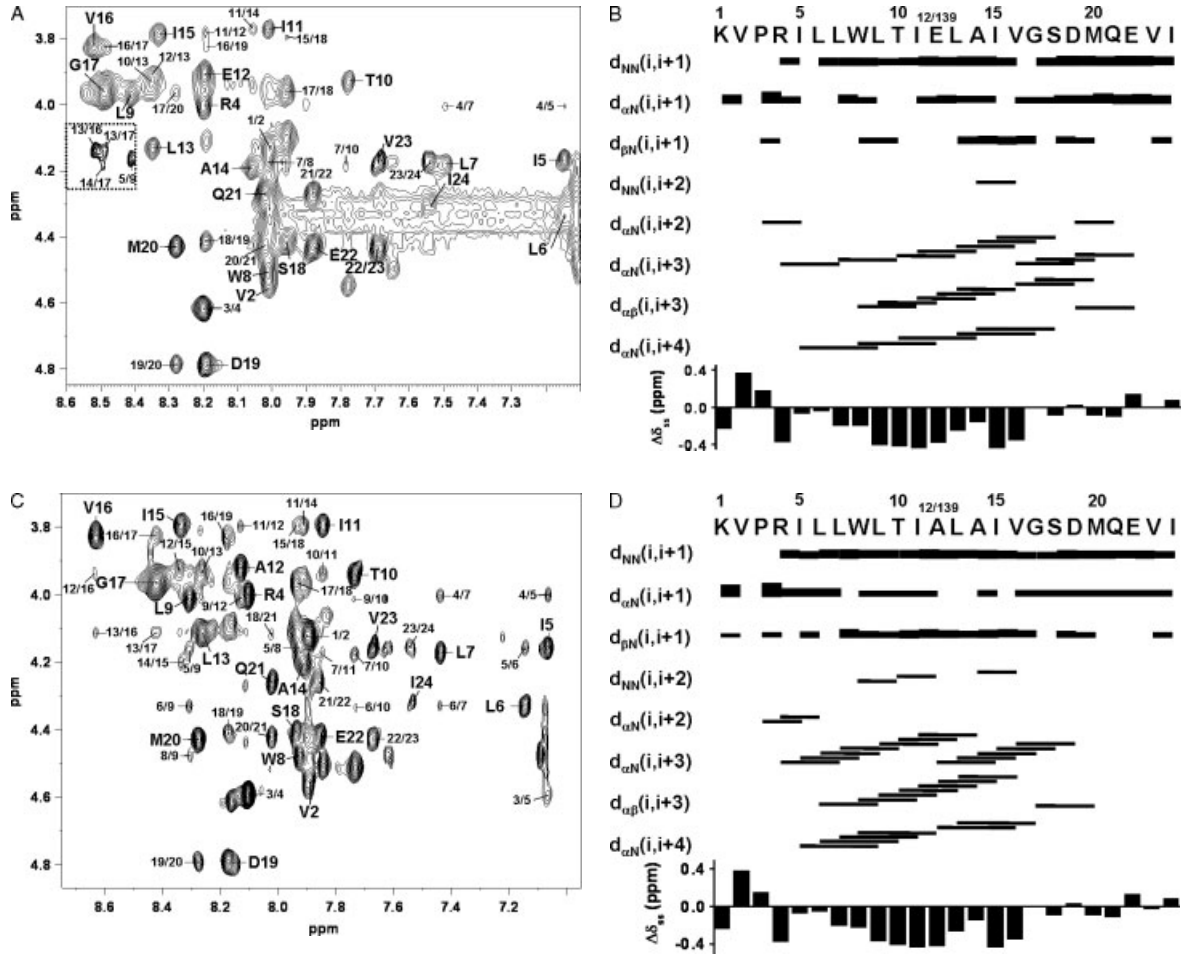

Figure 2. Hα-HN region of 2D NOESY spectra and NOE connectivities as well as secondary structure shifts for 2 mM WT peptide (A and B) and E139A mutant (C and D) at 310 K. The intensities of the cross-peaks closed with broken line are amplified three times as large as other cross-peaks in the figure.

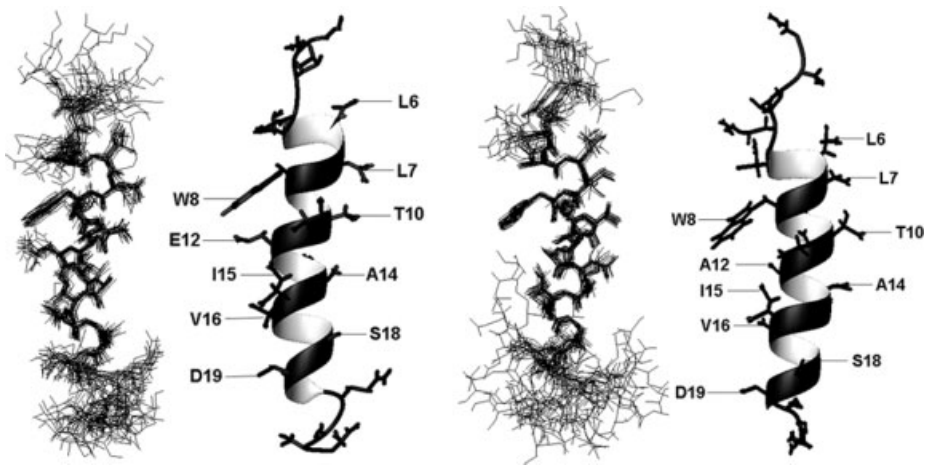

Figure 3. Ensemble of 20 structures with the lowest target functions and the ribbon representation of the mean structure for the WT peptide (left) and E139A mutant (right) at 310 K.

did not largely affect channel function of ORAI1, regardless of their charges [43]. For Slc11a1, the increase in hydrophobicity of TMD3 due to Glu139 substitution may change the relative position of the protein in the bilayer as well as its tilting and orientation, leading to a change in pore size of the channel. There may be other possibilities that could interpret the effect of glutamic acid replacement. By modeling SLC11 homologs on several template structures, Czachorowski *et al*. suggested that TMD1, 3, 6, and 8 construct a three-dimensional arrangement of the pathway that may play a key role in the transport mechanism [44]. If it is the case, the side chain of Glu139 may play a role in the metal ion transport, the Ala substitution may disrupt the

Journal of PeptideScience

Table 1. Structural statistics of the WT peptide and its E139A mutant at 310 K

Peptide	WT	E139A
Average target functions (Å^2)	0.09 ± 0.03	0.22 ± 0.02
Number of nonredundant distance restraints	226	239
Intraresidual ($\|i-j\|=0$)	114	120
Sequential ($\|i-j\|=1$)	58	64
Medium ($\|i-j\|\leq 4$)	54	55
Long range ($\|i-j\|>4$)	0	0
Average sum of distance restraint violations (Å)	0.6 ± 0.2	1.3 ± 0.2
Average maximum distance restraint violation (Å)	0.14 ± 0.03	0.16 ± 0.01
Average sum of torsion angle restraint violations (°)	1.5 ± 1.9	1.5 ± 1.8
Average maximum of torsion angle restraint violation (°)	1.52 ± 1.86	1.02 ± 1.19
AMBER energy (kcal mol^{-1})	−950.9 ± 0.8	−877.6 ± 0.4
Root mean square deviation from the mean structure (Å)		
All residues		
Backbone heavy atoms	1.59 ± 0.43	2.56 ± 0.92
All heavy atoms	2.30 ± 0.45	3.53 ± 0.98
Residues 5–19		
Backbone heavy atoms	0.47 ± 0.17	0.59 ± 0.22
All heavy atoms	1.13 ± 0.22	1.06 ± 0.29
Ramachandran plot statistics (at each helical span)		
Residues in most favored region (%)	94.6	98.2
Residues in additionally allowed region (%)	5.4	1.8
Residues in generously allowed region (%)	0	0
Residues in disallowed region (%)	0	0

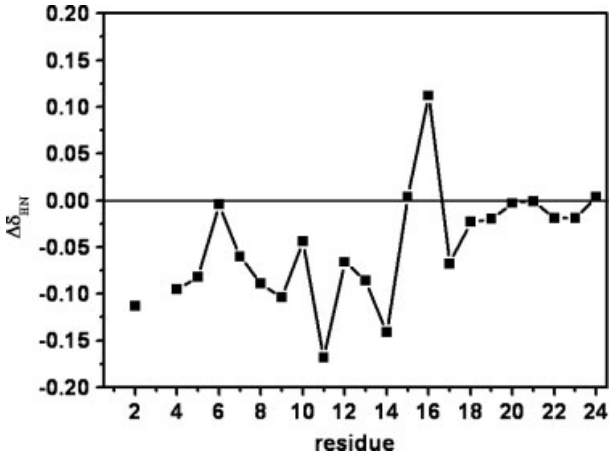

Figure 4. The HN chemical shifts of 2 mM E139A mutant relative to those of 2 mM WT peptide at 310 K.

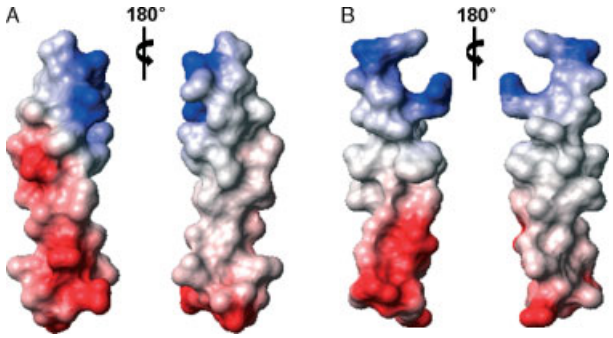

Figure 5. The electrostatic surface potential maps of the WT peptide (A) and its E139A mutant (B). The right view is rotated by 180° along the *y*-axis of the left view. Red, white, and blue colors represent negative, neutral, and positive electrostatic potential, respectively.

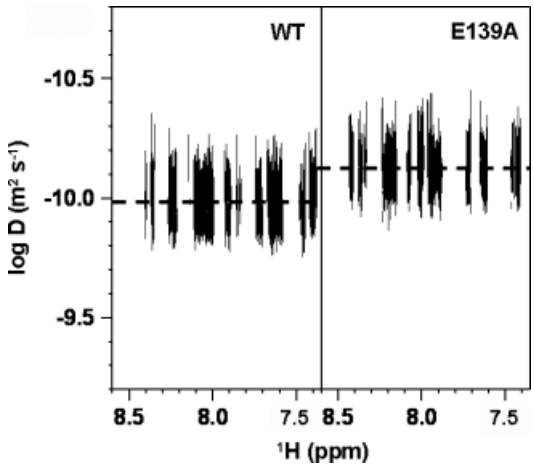

Figure 6. DOSY spectra of 2 mM WT peptide and E139A mutant at 298 K.

interactions between Glu139 and adjacent residues, causing loss of function.

Self-assembly

DOSY is an effective method for assessing the aggregation state of proteins. It provides a correlation between diffusion coefficient (*D*) and molecular size through Stokes–Einstein equation [45]. We used this method to assess the aggregate state of the WT peptide and its E139A mutant in 60% HFIP-d_2 aqueous solution at 298 K. The diffusion coefficients of peptide and H_2O in a sample were measured separately. The latter was used to correct the viscosity of solution. The DOSY spectra of 2 mM peptide are shown in Figure 6. The corresponding pairs of diffusion coefficients for peptide and H_2O were obtained to be 1.035×10^{-10} m^2 s^{-1} and 1.023×10^{-9} m^2 s^{-1} for the sample of WT peptide and 7.870×10^{-11} m^2 s^{-1} and 9.908×10^{-10} m^2 s^{-1} for the sample of E139A mutant, respectively. The molecular weights were therefore estimated according to Eqn (3) to be 2.65 kDa for the WT peptide and 5.47 kDa for the E139A mutant, corresponding to a monomer for the former (MW = 2.737 kDa for a single peptide) and a dimer for the latter (MW = 2.679 kDa for a single peptide). Dilution of the samples had little effect on the diffusion coefficients (data not shown). In the 2D NOESY and TOCSY spectra of E139A mutant, we only observed one set of resonances. Thus, we inferred that the peptide has dimerized with similar monomeric structure. Previous study demonstrated that small residues like Ser, Gly, Ala, and Thr are likely to be found at helix–helix interaction interfaces, frequently mediating tight helix–helix contacts and playing a critical role in maintaining the tertiary structure of helical membrane proteins

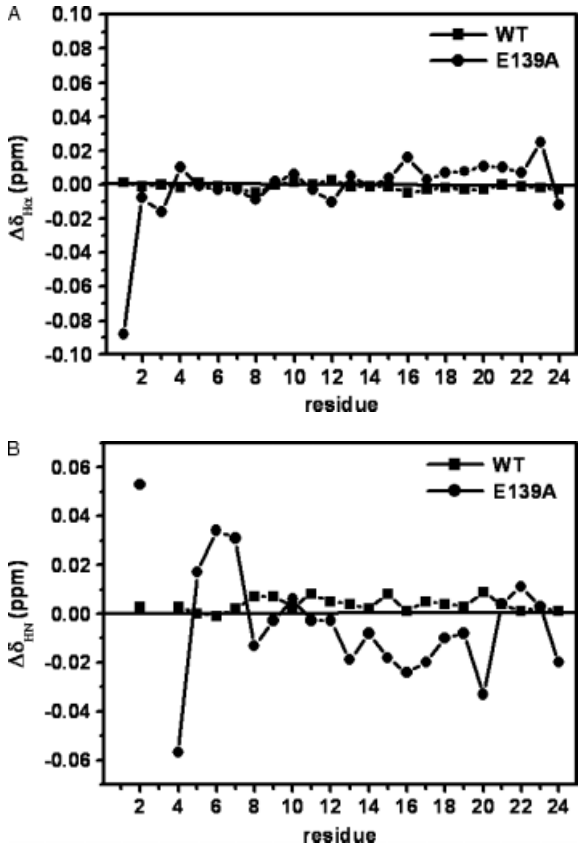

Figure 7. Hα (A) and HN (B) chemical shifts of 0.5 mM peptides relative to those of 2 mM peptides at 310 K.

[46]. Our data indeed indicated that the change from a negatively charged glutamic acid (Glu139) to a small apolar alanine enable a favorable interaction between monomers and assembly of TMD3.

From the NOESY and TOCSY spectra of the E139A mutant with the concentrations of 2 and 0.5 mM, we observed larger differences in HN chemical shifts of the residues Val2, Arg4-Leu7, Leu13, Ile15-Gly17, Met20, and Ile24, but the differences in the Hα chemical shifts were very small (Figure 7). Less shifting of the Hα resonances with dilution implies the similarity of both peptides in structure at the two concentrations. However, larger change in HN chemical shifts may imply more different intermolecular interactions in E139A dimer. The intermolecular interactions in the hydrophobic region of Trp8-Ala12 that display minimum resonance shifting with dilution may be relatively strong. This may evidence that the self-assembly of the E139A mutant is associated with increased hydrophobicity of the central part of the peptide.

Conclusion

The peptide from the TMD3 of Slc11a1 forms an amphipathic α-helical structure from Ile5 to Met20 in HFIP-d_2 aqueous solution with the charged residues being located on the same side of the helix, whereas hydrophobic residues occupying the opposite side. The E139A mutant also forms a helical structure in almost the same region to the WT peptide, but it is more hydrophobic and displays more tendentious to aggregate. Whereas the WT peptide exists as a monomer, the E139A mutant is associated to a dimer. The increase in hydrophobicity of the membrane-spanning peptide and/or change in the interactions between transmembrane segments induced by E139A mutation may alter orientation of the transmembrane segment that may affect the metal ion transport of the protein.

Acknowledgement

This work was financially supported by the NSFC (20973083 and 20934002).

References

1 Courville P, Chaloupka R, Cellier MF. Recent progress in structure-function analyses of Nramp proton-dependent metal-ion transporters. *Biochem. Cell Biol.* 2006; **84**: 960–978.
2 Gruenheid S, Gros P. Genetic susceptibility to intracellular infections: Nramp1, macrophage function and divalent cations transport. *Curr. Opin. Microbiol.* 2000; **3**: 43–48.
3 Cellier M, Privé G, Belouchi A, Kwan T, Rodrigues V, Chia W, Gros P. Nramp defines a family of membrane proteins. *Proc. Natl. Acad. Sci. U. S. A.* 1995; **92**: 10089–10093.
4 Cellier MF, Courville P, Campion C. Nramp1 phagocyte intracellular metal withdrawal defense. *Microbes Infect.* 2007; **9**: 1662–1670.
5 Vidal SM, Malo D, Vogan K, Skamene E, Gros P. Natural resistance to infection with intracellular parasites: isolation of a candidate for *Bcg*. *Cell* 1993; **73**: 469–485.
6 Vidal SM, Pinner E, Lepage P, Gauthier S, Gros P. Natural resistance to intracellular infections: *Nramp1* encodes a membrane phosphoglycoprotein absent in macrophages from susceptible (*Nramp1*^{D169}) mouse strains. *J. Immunol.* 1996; **157**: 3559–3568.
7 Mackenzie B, Hediger MA. SLC11 family of H^+-coupled metal-ion transporters NRAMP1 and DMT1. *Pflugers Arch.* 2004; **447**: 571–579.
8 Nevo Y, Nelson N. The NRAMP family of metal-ion transporters. *Biochim. Biophys. Acta* 2006; **1763**: 609–620.
9 Touret N, Martin-Orozco N, Paroutis P, Furuya W, Lam-Yuk-Tseung S, Forbes J, Gros P, Grinstein S. Molecular and cellular mechanisms underlying iron transport deficiency in microcytic anemia. *Blood* 2004; **104**: 1526–1533.
10 Gunshin H, Mackenzie B, Berger UV, Gunshin Y, Romero MF, Boron WF, Nussberger S, Gollan JL, Hediger MA. Cloning and characterization of a mammalian proton-coupled metal-ion transporter. *Nature* 1997; **388**: 482–488.
11 Makui H, Roig E, Cole ST, Helmann JD, Gros P, Cellier MF. Identification of the *Escherichia coli* K-12 Nramp orthologue (MntH) as a selective divalent metal ion transporter. *Mol. Microbiol.* 2000; **35**: 1065–1078.
12 Kehres DG, Zaharik ML, Finlay BB, Maguire ME. The NRAMP proteins of *Salmonella typhimurium* and *Escherichia coli* are selective manganese transporters involved in the response to reactive oxygen. *Mol. Microbiol.* 2000; **36**: 1085–1100.
13 Chaloupka R, Courville P, Veyrier F, Knudsen B, Tompkins TA, Cellier MF. Identification of functional amino acids in the Nramp family by a combination of evolutionary analysis and biophysical studies of metal and proton cotransport *in vivo*. *Biochemistry* 2005; **44**: 726–733.
14 Haemig HA, Brooker RJ. Importance of conserved acidic residues in MntH, the Nramp homolog of *Escherichia coli*. *J. Membr. Biol.* 2004; **201**: 97–107.
15 Nelson N, Sacher A, Nelson H. The significance of molecular slips in transport systems. *Nat. Rev. Mol. Cell Biol.* 2002; **3**: 876–881.
16 Agranoff D, Monahan IM, Mangan JA, Butcher PD, Krishna S. *Mycobacterium tuberculosis* expresses a novel pH-dependent divalent cation transporter belonging to the Nramp family. *J. Exp. Med.* 1999; **190**: 717–724.
17 Vidal S, Tremblay ML, Govoni G, Gauthier S, Sebastiani G, Malo D, Skamene E, Olivier M, Jothy S, Gros P. The Ity/Lsh/Bcg locus: natural resistance to infection with intracellular parasites is abrogated by disruption of the Nrampl gene. *J. Exp. Med.* 1995; **182**: 655–666.
18 Martínez-Barnetche J, García Solache M, Neri Lecona A, Tello López AT, del Carmen Rodríguez M, Gamba G, Vázquez N, Rodríguez MH, Lanz-Mendoza H. Cloning and functional characterization of the Anopheles albimanus DMT1/NRAMP

homolog: implications in iron metabolism in mosquitoes. *Insect Biochem. Mol. Biol.* 2007; **37**: 532–539.
19 Fleming MD, Romano MA, Su MA, Garrick LM, Garrick MD, Andrews NC. Nramp2 is mutated in the anemic Belgrade (*b*) rat: evidence of a role for Nramp2 in endosomal iron transport. *Proc. Natl. Acad. Sci. U. S. A.* 1998; **95**: 1148–1153.
20 Lam-Yuk-Tseung S, Govoni G, Forbes J, Gros P. Iron transport by Nramp2/DMT1: pH regulation of transport by 2 histidines in transmembrane domain 6. *Blood* 2003; **101**: 3699–3707.
21 Gerig JT. Structure and solvation of melittin in 1,1,1,3,3,3-hexafluoro-2-propanol/water. *Biophys. J.* 2004; **86**: 3166–3175.
22 Hirota N, Mizuno K, Goto Y. Group additive contributions to the alcohol-induced α-helix formation of melittin: implication for the mechanism of the alcohol effects on proteins. *J. Mol. Biol.* 1998; **275**: 365–378.
23 Walgers R, Lee TC, Cammers-Goodwin A. An indirect chaotropic mechanism for the stabilization of helix conformation of peptides in aqueous trifluoroethanol and hexafluoro-2-propanol. *J. Am. Chem. Soc.* 1998; **120**: 5073–5079.
24 Díaz MD, Fioroni M, Burger K, Berger S. Evidence of complete hydrophobic coating of bombesin by trifluoroethanol in aqueous solution: an NMR spectroscopic and molecular dynamics study. *Chem. Eur. J.* 2002; **8**: 1663–1669.
25 Crescenzi O, Tomaselli S, Guerrini R, Salvadori S, D'Ursi AM, Temussi1 PA, Picone D. Solution structure of the Alzheimer amyloid β-peptide (1–42) in an apolar microenvironment. *Eur. J. Biochem.* 2002; **269**: 5642–5648.
26 Goddard TD, Kneller DG. *SPARKY 3*. University of California: San Francisco, CA, 2001.
27 Güntert P, Mumenthaler C, Wüthrich K. Torsion angle dynamics for NMR structure calculation with the new program DYANA. *J. Mol. Biol.* 1997; **273**: 283–298.
28 Pearlman DA, Case DA, Caldwell JW, Ross WS, Cheatham TE, Debolt S, Ferguson D, Seibel G, Kollman P. AMBER, a package of computer programs for applying molecular mechanics, normal mode analysis, molecular dynamics and free energy calculations to simulate the structural and energetic properties of molecules. *Comput. Phys. Commun.* 1995; **91**: 1–41.
29 Cornell WD, Cieplak P, Bayly CI, Gould IR, Merz KM, Jr, Ferguson DM, Spellmeyer DC, Fox T, Caldwell JW, Kollman PA. A second generation force field for the simulation of proteins, nucleic acids, and organic molecules. *J. Am. Chem. Soc.* 1995; **117**: 5179–5197.
30 Case DA, Pearlman DA, Caldwell JW, Cheatham TE, III, Wang J, Ross WS, Simmerling CL, Darden TA, Merz KM, Stanton RV, Cheung AI, Vincent JJ, Crowley M, Tsui V, Gohike H, Radmer RJ, Duan Y, Pitera J, Massova I, Seibel GL, Singh UC, Weiner PK, Kollman PA. *AMBER 7*. University of California: San Francisco, CA, 2002.
31 Laskowski RA, Rullmann JA, MacArthur MW, Kaptein R, Thornton JM. AQUA and PROCHECK-NMR: programs for checking the quality of protein structures solved by NMR. *J. Biomol. NMR* 1996; **8**: 477–486.
32 Koradi R, Billeter M, Wüthrich K. MOLMOL: a program for display and analysis of macromolecular structures. *J. Mol. Graph* 1996; **14**: 51–55.
33 Eisenberg D, Kauzmann W. *The Structure and Properties of Water*. Oxford University Press: London, 1969.
34 Cho CH, Urquidi J, Singh S, Wilse Robinson G. Thermal offset viscosities of liquid H_2O, D_2O, and T_2O. *J. Phys. Chem. B* 1999; **103**: 1991–1994.
35 Yao S, Howlett GJ, Norton RS. Peptide self-association in aqueous trifluoroethanol monitored by pulsed field gradient NMR diffusion measurements. *J. Biomol. NMR* 2000; **16**: 109–119.
36 Perkins SJ. Protein volumes and hydration effects. The calculations of partial specific volumes, neutron scattering matchpoints and 280-nm absorption coefficients for proteins and glycoproteins from amino acid sequences. *Eur. J. Biochem.* 1986; **157**: 169–180.
37 Fioroni M, Burger K, Mark AE, Roccatano D. Model of 1,1,1,3,3,3-hexafluoro-propan-2-ol for molecular dynamics simulations. *J. Phys. Chem. B* 2001; **105**: 10967–10975.
38 Cantor CR, Schimmel PR. *Biophysical Chemistry, Part II: Techniques for the Study of Biological Structure and Function*. W. H. Freeman: New York, 1980; 539–590.
39 Epand RM. *The Amphipathic Helix*. CRC Press, Inc.: Florida, 1993.
40 Bechinger B. Structure and functions of channel-forming peptides: magainins, cecropins, melittin and alamethicin. *J. Membr. Biol.* 1997; **156**: 197–211.
41 Thompson AN, Posson DJ, Parsa PV, Nimigean CM. Molecular mechanism of pH sensing in KcsA potassium channels. *Proc. Natl. Acad. Sci. U. S. A.* 2008; **105**: 6900–6905.
42 Sahin-Toth M, Dunten RL, Gonzales A, Kaback HR. Functional interactions between putative intramembrane charged residues in the lactose permease of *Escherichia coli*. *Proc. Natl. Acad. Sci. U. S. A.* 1992; **89**: 10547–10551.
43 Derler I, Fahrner M, Carugo O, Muik M, Bergsmann J, Schindl R, Frischauf I, Eshaghi S, Romanin C. Increased hydrophobicity at the N-terminus/membrane interface impairs gating of the SCID-related ORAI1 mutant. *J. Biol. Chem.* 2009; **284**: 15903–15915.
44 Czachorowski M, Lam-Yuk-Tseung S, Cellier M, Gros P. Transmembrane topology of the mammalian Slc11a2 iron transporter. *Biochemistry* 2009; **48**: 8422–8434.
45 Altieri AS, Hinton DP, Andrew Byrd R. Association of biomolecular systems via pulsed field gradient NMR self-diffusion measurements. *J. Am. Chem. Soc.* 1995; **117**: 7566–7567.
46 Eilers M, Shekar SC, Shieh T, Smith SO, Fleming PJ. Internal packing of helical membrane proteins. *Proc. Natl. Acad. Sci. U. S. A.* 2000; **97**: 5796–5801.

